Natural Convection of Air Layers in Vertical Annuli with Cooled Outer Wall

Shou-Shing Hsieh,* Wen-San Han,† and Shyi-Ching Lin†
National Sun Yat-Sen University, Kaohsiung, Taiwan, Republic of China

Temperature measurement is presented for natural convection of air layers in vertical annuli wherein the inner cylinder is at constant surface heat flux and the outer cylinder is cooled. In this paper, flow visualization was made and discussed for different Rayleigh numbers and aspect ratios. Temperature data were taken for Rayleigh numbers $10^3 \le Ra \le 8 \times 10^5$, radius ratios $3.5 \le K \le 9.86$, and aspect ratios $10.65 \le H \le 37.71$. The resulting Nusselt number correlations are represented by the conduction regime $Nu = 0.840\ Ra^{0.106}$ for $H = 37.71$ and $K = 3.5$ and the boundary layer regime $Nu = 0.191\ Ra^{0.3204}\ H^{-0.121}$ for $10.65 \le H \le 37.71$ and $3.50 \le K \le 9.86$. The results of the present study may provide basic heat-transfer data for convection Nusselt number. Furthermore, with a modified thermal boundary-layer thickness proposed, a scale analysis was made for thermal correlation as a function of Rayleigh number and geometrical parameters, which also qualitatively validates the present experiments.

Nomenclature

c_p = specific heat at constant pressure, J/kgK
g = gravitational acceleration, m/s^2
Gr = Grashof number, $g\beta\Delta T\ell^3/\nu^2$
h = convective heat transfer coefficient, $q_c/\Delta T$, W/m^{2}K
H = aspect ratio of cylinder, L/ℓ
k = thermal conductivity, W/mK
K = radius ratio, r_o/r_i
ℓ = length scale, $r_o - r_i$, m
L = height of annulus or layer, m
Nu = average Nusselt number based on gap, $h\ell/k$
Pr = Prandtl number, ν/α
q_c = heat flux based on inner cylinder area, W/m^2
r = radius, m
Ra = Rayleigh number, $GrPr$
T = temperature, K
T_f = mean temperature of the fluid, $(\bar{T}_i + \bar{T}_o)/2$, K
z = vertical coordinate, m
ΔT = characteristic temperature difference, $\bar{T}_i - \bar{T}_o$, K
α = thermal diffusivity, m^2/s
β = thermal expansion coefficient, 1/K
ν = kinematic viscosity, m^2/s
ρ = density, kg/m^3
δ = boundary-layer thickness, m

Subscripts

i = inner wall
o = outer wall
$-$ = mean value

Introduction

THIS paper presents results of an experimental study of free convection in vertical annuli where the inner wall provides constant heat flux and the cooled outer wall loses heat to the ambient. The present study extends the work of Keyhani et al.[1] and Bhushan et al.[2] Additionally, flow visualization was conducted to observe the flowfield at different Rayleigh numbers and aspect ratios. The present results, in combination with results of previous studies, can therefore serve to provide a limiting-case correlation for heat transfer from a nuclear fuel rod bundle to the interior of its canister in either storage or disposal.

Before describing the present experiments, it must be pointed out that the correlation for the thermal boundary conditions and geometrical parameters of this work has not been treated before. However, several relevant works may still be referred. For a vertical annulus with both walls at constant temperature, the numerical works of de Vahl Davis and Thomas[3] and Thomas and de Vahl Davis[4] and the experimental work of Nagendra et al.[5] provide results for Nusselt numbers and flowfields that can serve as the basis for qualitative comparison with the results of the present work. De Vahl Davis and Thomas[3] have performed finite-difference calculations of free convection in a vertical annulus for $0.5 \le Pr \le 5$, $1 \le K \le 4$, $1 \le H \le 20$, and $Ra \le 2 \times 10^5$, and results for laminar axisymmetric flows were for $Pr = 1$. For $Ra < 10^5$, unicellular flow exists, while at larger Ra, multicellular flow was observed. Local heat-transfer coefficients on the inner wall were found to increase with an increase in the radius ratio but to decrease with increasing aspect ratio. Moreover, three regimes of heat transfer have been identified (conduction, transition, and boundary-layer regimes), with the structure of the flowfield in each regime dependent on Ra.[3,4] Heat-transfer correlations for the average Nusselt numbers developed by Thomas and de Vahl Davis are given by

Conduction regime:

$$Nu = 0.595 Ra^{0.101} Pr^{0.024} H^{-0.052} K^{0.505}$$

Transition regime:

$$Nu = 0.202 Ra^{0.294} Pr^{0.097} H^{-0.264} K^{0.423}$$

Boundary-layer regime:

$$Nu = 0.286 Ra^{0.258} Pr^{0.006} H^{-0.238} K^{0.442}$$

These correlations were developed for $1 \le K \le 10$, $1 \le H \le 33$, $0.5 \le Pr \le 10^4$, and $Ra \le 2 \times 10^5$. The experimental work of Sheriff[6] considered natural convection in a vertical annulus with constant heat flux on the inner wall, while the outer wall was kept at constant temperature. The working fluid was carbon dioxide, pressurized to extend the range of Rayleigh numbers.

Received Jan. 4, 1988; revision received April 26, 1988.

*Associate Professor, Department of Mechanical Engineering. Member AIAA.
†Graduate Student, Department of Mechanical Engineering.

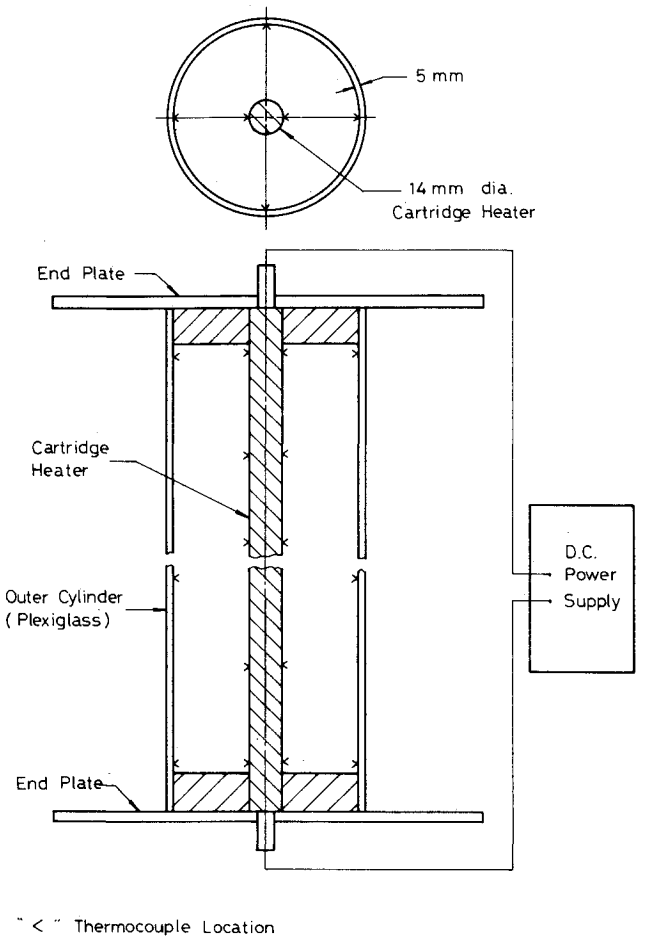

Fig. 1 Schematic of experimental apparatus and instrumentation.

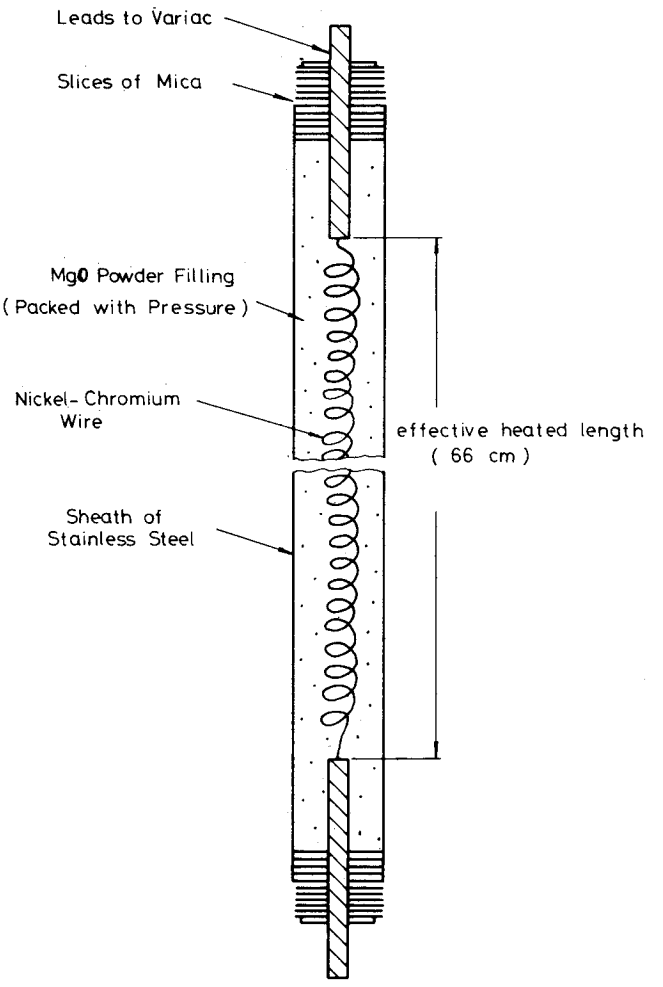

Fig. 2 Details of heated rod.

Choi and Korpela[7] studied the stability of natural convection in a vertical annulus enclosure by the linear theory, and the theoretical predictions of the mode of instability were verified for air through flow visualization. Recently, flow visualization was experimented by Figliola[8] for a bounded vertical cylinder heated from beneath using a high Prandtl number fluid for Rayleigh numbers up to 11,800. He suggests that axisymmetric motion of the toroidal type is possible between Rayleigh numbers of 4150 and 120,000. The onset of convection, the critical Rayleigh number, was observed at 4150, with the appearance of an axisymmetric motion.

Experimental Apparatus and Procedure

The major components of the experimental apparatus consisted of the outer cylinder, and plates, heater rod, and power supply, with associated controls and instrumentation. Figure 1 presents a schematic of the apparatus and instrumentation. The inner cylinder was a cartridge heater of 14-mm diam. with an effective heating length of 660 mm, as shown in Fig. 2, and was designed to provide uniform power dissipation per unit length. It comprises a nickel-chromium wire wound around a magnesium oxide core with a 0.05-cm sheath of stainless steel. Two 0.625-cm-thick pieces of square stainless steel plates with a side length of 30 cm formed the end plates. A 1.45-cm-diam threaded hole on each geometrical center of end plates was drilled for mounting the heating rod. The ends of the annulus were insulated with 2 cm of Plisulate. Fourteen equally spaced thermocouples, tapped to the inner-cylinder surface, were used to measure the temperature along the inner cylinder, and 20 equally spaced thermocouples were potted into 0.35-cm-deep holes drilled through the outside surface to measure temperatures along the inner surface of the outer cylinder. To facilitate the flow visualization, the outer cylinder was made of 710-mm-tall plexiglass with varied inside diameter, and to attain a better visual effect, the surface of the inner cylinder was painted with a very thin black dye layer ($\sim 10\ \mu$m). The positions and arrangements of these thermocouples are shown in Fig. 1.

The electrical circuit consisted of a 0–30 V and 0–3 A dc power supply, connected in series with the heated rod, a precision resistor, and a variable resistance to produce the thermal input rate from 1.12–28.24 W. Power is held to within $\pm 1\%$ of the set value under normal conditions. Temperature data were recorded with an HP 3054 + 85B PC multichannel datalogger.

Flow visualization was done for the height-to-width ratio H of 37.7 with the corresponding radius ratio k of 3.5 and for the height-to-width ratio H of 10.65 with the corresponding radius ratio K of 9.86. The somewhat larger radius ratio for the plexiglass cylinder is expected not to affect the flowfield significantly. Gross flow features were visualized by injecting a few grams of aluminum powder with neutrally buoyant suspended aluminum particles of nominal 5-μm diam through several 1-mm holes. The illumination of the particles was done by using a slide projector as a light source shining through a narrow slit so as to produce a plane of light. The flow was allowed to reach a steady-state condition prior to illumination with the light sources. It usually takes 11 h to reach a steady state. All photographs were taken with a Canon-AE1 camera on Konica SR 1600 film with exposure times of 1/2–1/15 s. It appears that none of the existing studies has discussed the refraction of the circular cylinder filled with fluid.[7,8] Therefore, one may consider that it is not expected to affect the visualization result significantly.

The thermophysical properties for the testing fluid (i.e., air) were considered to vary with temperature. In the calculation of Ra and Nu, using the temperature difference between the mean temperature of the inner and outer wall ($\Delta T = \bar{T}_i - \bar{T}_o$), fluid

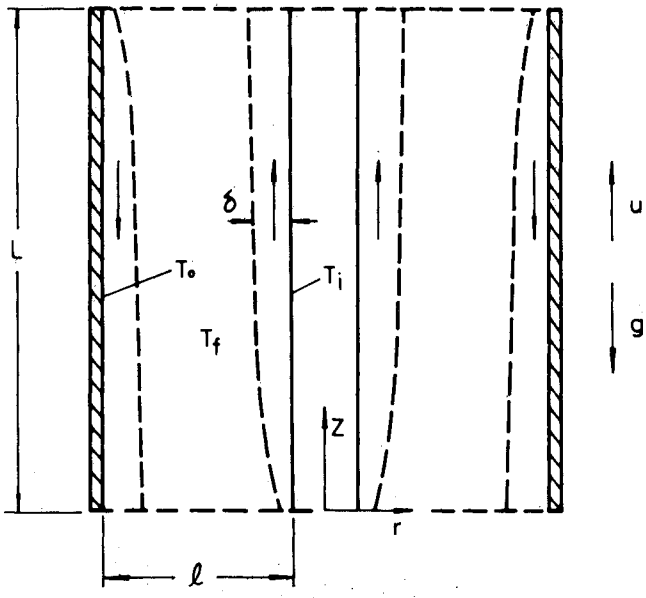

Fig. 3 Physical model for vertical annuli.

properties were evaluated at the temperature $T_f = (\bar{T}_i + \bar{T}_o)/2$. Experimental uncertainties in Ra and Nu were 2–12% and 6–16%, respectively. These uncertainties represent the maximum uncertainty based on the absolute value of individual uncertainties. End losses via conduction along the heated cylinder were estimated to be about 0.5–1.5% of the applied power by making a comparison of thermal resistances in the vertical direction with that in the radial direction.

Scale Analysis

Following the sketch of the thermal boundary layer in Fig. 3 and the book written by Bejan,[9] a scale analysis was made to incorporate the correlation obtained by the experimental data. Consider a two-dimensional vertical annulus of height L and annulus thickness ℓ, as indicated in Fig. 3. The enclosure is filled with a Newtonian fluid such as air. With Boussinesq approximation assumed, the equations governing the conservation of mass, momentum, and energy at every point in the enclosure are

$$\frac{v}{r} + \frac{\partial v}{\partial r} + \frac{\partial u}{\partial z} = 0 \tag{1}$$

$$v\frac{\partial v}{\partial r} + u\frac{\partial v}{\partial z} = -\frac{1}{\rho}\frac{\partial P}{\partial r} + \nu\left[\frac{1}{r}\frac{\partial}{\partial r}\left(r\frac{\partial v}{\partial r}\right) + \frac{\partial^2 v}{\partial z^2} - \frac{v}{r^2}\right] \tag{2}$$

$$v\frac{\partial u}{\partial r} + u\frac{\partial u}{\partial z} = -\frac{1}{\rho}\frac{\partial p}{\partial z} + g\beta(T - T_o) + \nu\left[\frac{1}{r}\frac{\partial}{\partial r}\left(r\frac{\partial u}{\partial r}\right) + \frac{\partial^2 u}{\partial z^2}\right] \tag{3}$$

$$v\frac{\partial T}{\partial r} + u\frac{\partial T}{\partial z} = \alpha\left[\frac{1}{r}\frac{\partial}{\partial r}\left(r\frac{\partial T}{\partial r}\right) + \frac{\partial^2 T}{\partial z^2}\right] \tag{4}$$

Eliminating the pressure P between the two momentum equations [(2) and (3)], yields

$$\frac{\partial}{\partial r}\left(v\frac{\partial u}{\partial r} + u\frac{\partial u}{\partial z}\right) - \frac{\partial}{\partial z}\left(v\frac{\partial v}{\partial r} + u\frac{\partial v}{\partial z}\right) = \frac{\partial}{\partial r}[g\beta(T - T_0)] + \nu\left\{\frac{\partial}{\partial r}\left[\frac{1}{r}\frac{\partial}{\partial r}\left(r\frac{\partial u}{\partial r}\right) + \frac{\partial^2 u}{\partial z^2}\right] - \frac{\partial}{\partial z}\left[\frac{1}{r}\frac{\partial}{\partial r}\left(r\frac{\partial v}{\partial r}\right) + \frac{\partial^2 v}{\partial z^2} - \frac{v}{r^2}\right]\right\} \tag{5}$$

Equation (5) contains three basic groups of terms—the inertia term on the left-hand side and four viscious diffusion terms plus the buoyancy term on the right-hand side. In terms of representative scales, Eq. (5) reads

$$\frac{u^2}{L}, \quad \frac{vu}{\delta^2}, \quad g\beta\Delta T \tag{6}$$

Following the same procedure with the assumption of $\delta \sim \Delta$, the energy equation (4) becomes

$$\frac{u\Delta T}{L} \sim \alpha\frac{\Delta T}{\delta^2} \tag{7}$$

Here, we proposed a modified thermal boundary layer thickness $\delta(L/\delta)^{1/4}$ to replace the initial δ. This is due to the curvature effect of the present physical geometry. The amplification factor $(L/\delta)^{1/4}$ was not derived from the mathematics. It solely depends on the present experimental data and phenomenological behavior. Substituting this modified thermal boundary–layer thickness into Eq. (7), we conclude that the vertical velocity scale is

$$u \sim \alpha\frac{L}{\delta^2}\left(\frac{\delta}{L}\right)^{1/2} \tag{8}$$

Inserting Eq. (7) into Eq. (8), one finds

$$\left(\frac{L}{\delta}\right)^3 Pr^{-1} \text{ or } \left(\frac{L}{\delta}\right)^{7/2} \sim \frac{g\beta\Delta T}{\alpha\nu}L^3 \tag{9}$$

Therefore, for fluids with Prandtl number of order one or greater, the correct momentum balance is between buoyancy and friction. Therefore Eq. (9) becomes

$$L/\delta \sim L/\ell^{6/7}Ra^{2/7} \tag{10}$$

where $\ell = r_o - r_i$. By definition, the average Nusselt number is

$$Nu = \frac{\dfrac{q_c}{\Delta T}\ell}{K} \tag{11}$$

Since

$$q_c \sim k\frac{\bar{T}_i - T_f}{\delta}$$

where

$$T_f = (\bar{T}_i + \bar{T}_o)/2, \ \bar{T}_i - \bar{T}_f = \Delta T/2$$

Eq. (11) yields

$$Nu \sim H^{-1/7}Ra^{2/7} \tag{12}$$

Based on the derivation, Eq. (12) is marginally valid for air ($Pr \sim 1$).

Results and Discussion

The fluid motion development was recorded over time until a steady pattern resulted. This motion was detected initially near the top end of the test apparatus in the form of an axisymmetric toroidal cell that is not shown here. In Fig. 4, the results reported are for $Pr = 0.7$ at $Ra = 5.3 \times 10^3$, 8.45×10^3, and 1.37×10^4. Flowfields are given for the top, below the midheight, and the bottom of cylinder, with three different Grashof numbers. For $Gr = 7571$, the flow consists of cells at the top end of the enclosures. This characteristic becomes distinct as Gr increases. The second photograph corresponds to the flow in the conduction regime for $Gr = 12{,}000$ before the onset of instability. As the Grashof number is increased to 20,000, it is seen that the flow becomes more irregular below the midheight of the cylinder. However, the shapes of the cells for the flow in the last photograph seems similar to those in the first photograph.

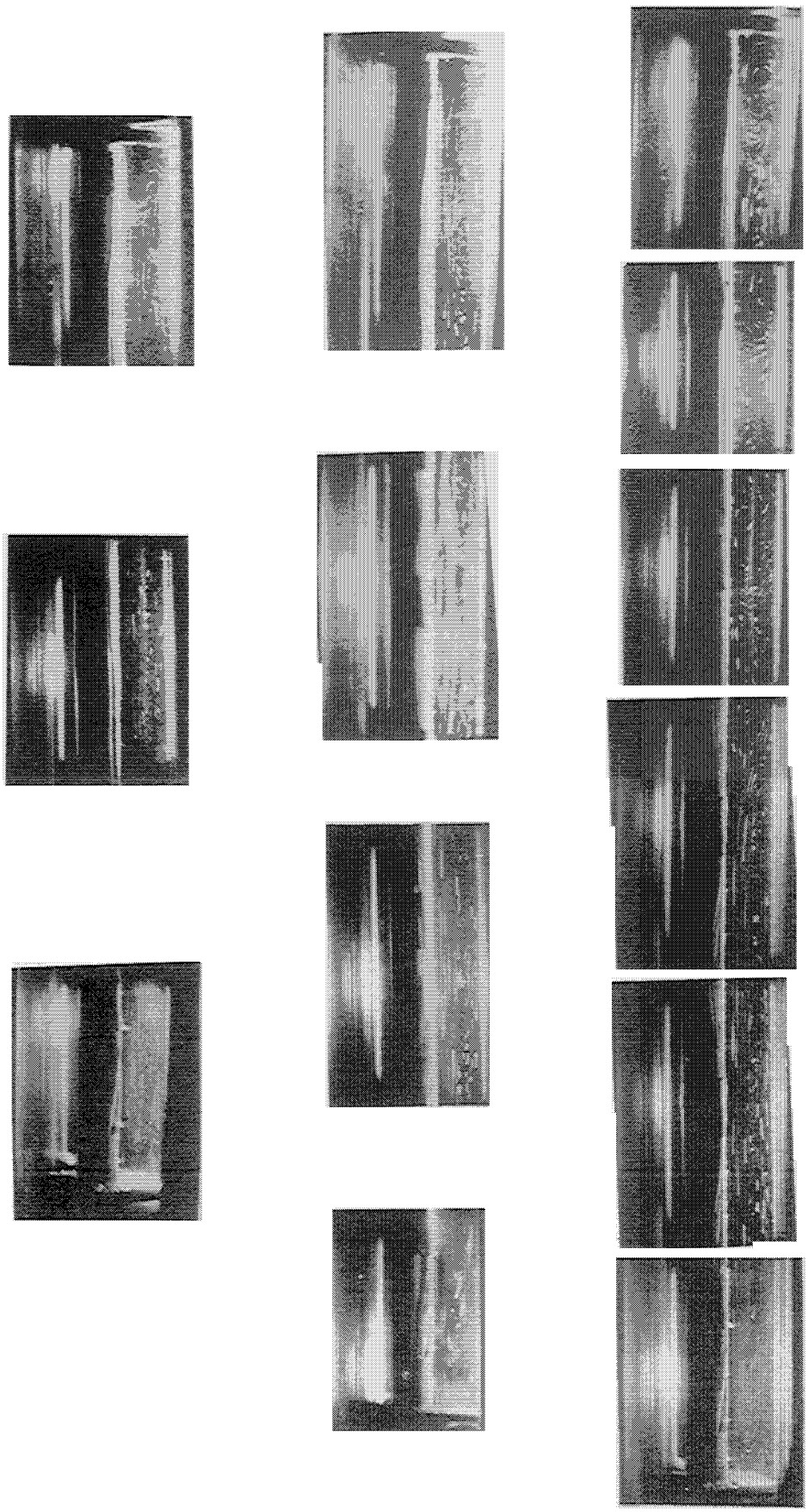

$Ra = 5.3 \times 10^3$
$Gr = 7571$

$Ra = 8.45 \times 10^3$
$Gr = 12{,}000$

$Ra = 1.37 \times 10^4$
$Gr = 20{,}000$

Fig. 4 Flowfield in vertical annuli with $H = 37.71$, $K = 3.50$ for $Ra = 5.3 \times 10^3$, 8.45×10^3, and 1.37×10^4.

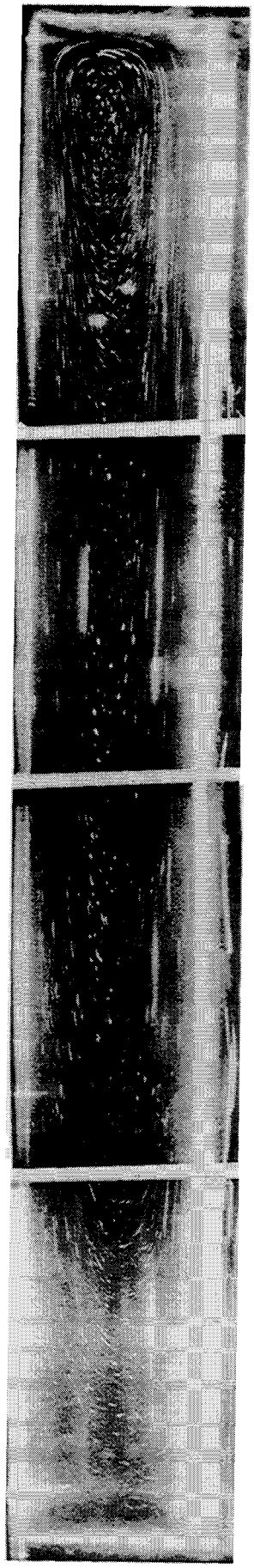

Fig. 5 Flowfield in vertical annuli with $H = 10.65$, $K = 9.86$ for $Ra = 2.19 \times 10^5$.

Fig. 6 Flowfield in vertical annuli with $H = 10.65$, $K = 9.86$ for $Ra = 6.7 \times 10^5$.

Two more sets of photographs are included for $H = 10.65$ and $K = 9.86$. For $Ra = 2.19 \times 10^5$, Fig. 5, it seems that the flow is still in the boundary-layer regime. As Ra is increased to 6.7×10^5, the flow, as expected, becomes more irregular, as can be seen from Fig. 6.

The major results of the flow visualization are that for lower K, when the cells reach either the top or bottom end region, they are quickly destroyed. Away from the ends, the flow is mainly vertical, with a slight periodic variation in the amplitude of the vertical velocity. This periodicity of vertical velocity together with that of a small transverse component generates the cellular stream pattern. Upon reaching the ends, the main flow becomes two-dimensional and the cells disappear. The resultant streamlines in the end region are only slightly distorted from what they would be if cells were not present. This finding is based not only on the current observations of the flow but on the previous experimental work reported by Choi and Korpela.[7]

Results obtained in the present work include temperature distributions on the surface of the heating rod and heat-transfer coefficients for natural convection and combined natural convection and thermal radiation for Rayleigh numbers from 10^3–8×10^5. This range of Rayleigh numbers spans the conduction regime to the boundary-layer regime of convection, as defined in the study of Thomas and de Vahl Davis[4] and based on the current flow visualization. In all experimental runs, conduction heat losses along the inner cylinder through the end plates were first deducted from thermal input rates, and then a correction for thermal radiation in the annulus was applied in the calculation of the coefficient for natural convection. This correction includes the effects of surface emissivities and radiative view factors. The correction for thermal radiation was estimated by using the simple calculation from Ref. 10. Through the calculation, one found that C_r defined in Ref. 1 without taking conduction heat loss into account, has values in the present systems from 0.93–0.96 for $H = 37.7$–10.65 and mean temperatures of the air from 300–400 K.

Figure 7 shows the difference of mean temperatures on the inner and outer walls of the annulus as a function of total rod power of $3.50 \le K \le 9.86$ and $10.65 \le H \le 37.71$. The tendency is similar to that of Kayhani et al.[1] However, for the three different geometries, it is interesting to see that the distribution is almost independent of the geometry of the present annular configuration at thermal power rates below 10 W. For higher thermal power rates (≥ 10 W), the deviation of the mean temperature difference across the annulus for these three different geometries can be clearly noted. Figure 8 displays the temperature distributions on the inner cylinder as a function of rod power. The accuracy of the temperature measurement was ± 1°C, which is reflected in the size of the data point. In this figure, the temperature distribution exhibits an almost constant feature at low rates of power, and this behavior becomes more apparent as the rate of power further decreases, which agrees well with that of Keyhani et al.[1] for the same inner boundary condition. But at higher rates of power, an asymmetrical distribution is observed. The temperature increases with increasing distance from the bottom, indicating a thickening of the thermal boundary layer at the top of the annulus. It appears that the flowfield of $10^3 \le Ra \le 10^4$ is most probably unicellular at low thermal power rates and is dominated by a well-mixed core and thermal boundary layers on each wall at higher thermal power rates for $Ra \ge 10^5$. In fact, this conclusion was verified by the flow visualization in the present work.

Overall Nusselt number as a function of Ra is presented in Figs. 9 and 10. The current results permit the identification of only two regimes of heat transfer for $H = 37.71$ and $K = 3.50$

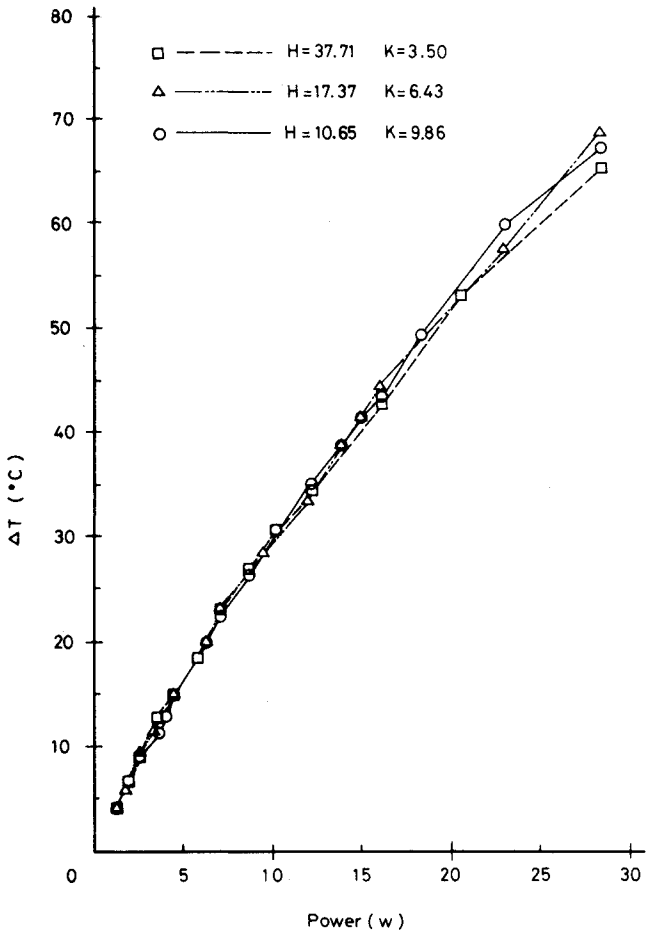

Fig. 7 Temperature difference across the annulus as a function of total rod power.

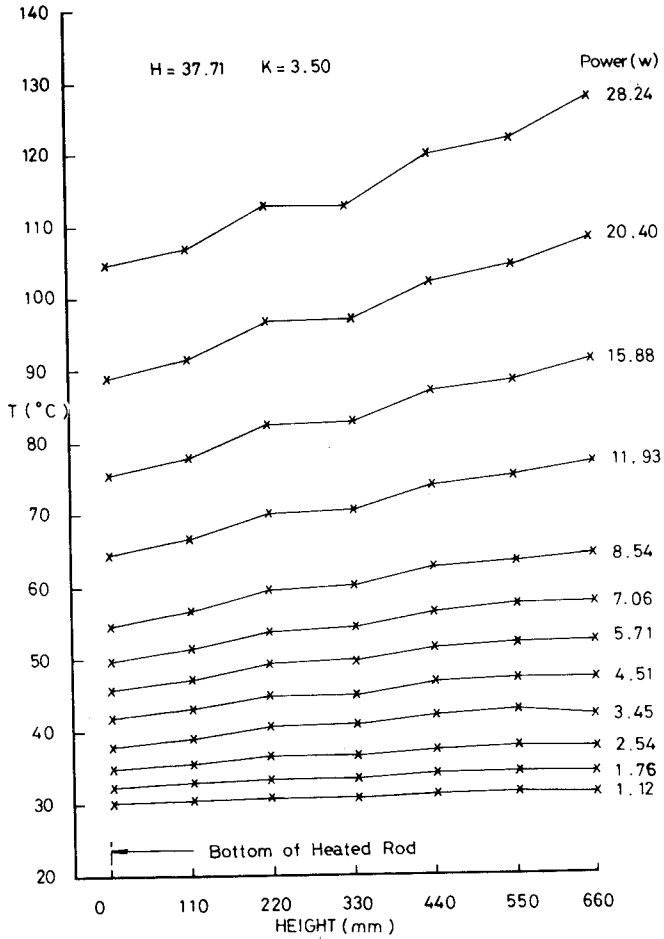

Fig. 8 Temperature distribution on the rod surface for $H = 37.71$, $K = 3.50$.

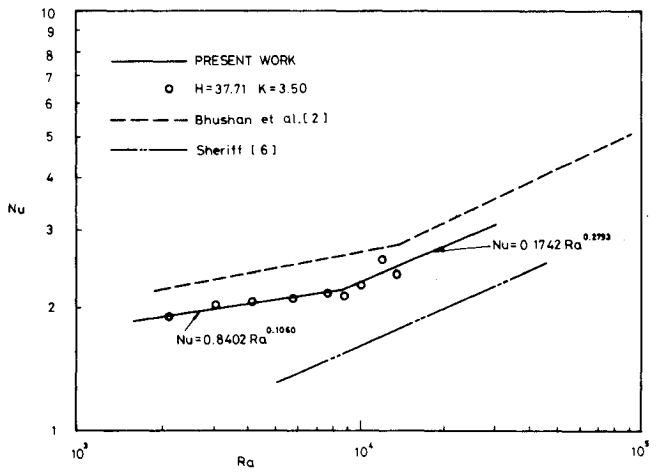

Fig. 9 Average Nusselt number as a function of Rayleigh number, and comparison with Bhushan et al.[2] and Sheriff[6] for $H = 37.71$ and $K = 3.5$.

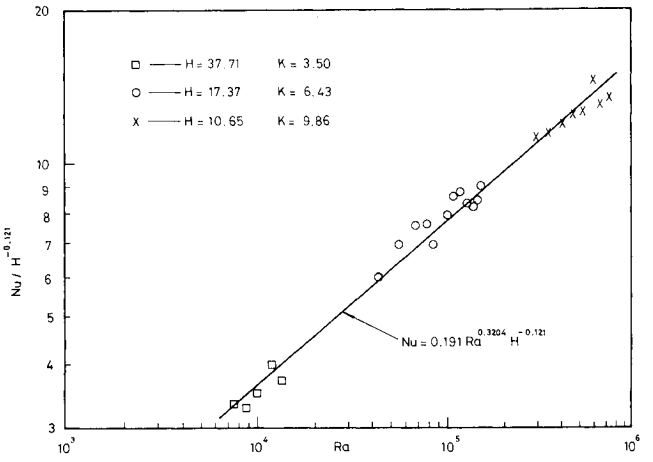

Fig. 11 Correlation of Nusselt number with Rayleigh number and aspect ratio.

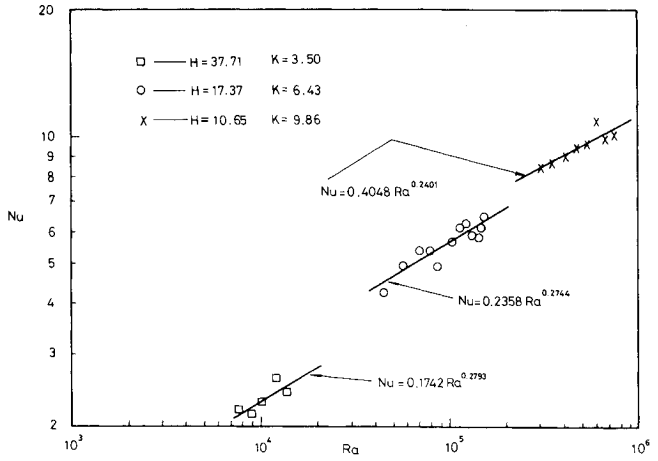

Fig. 10. Average Nusselt number as a function of Rayleigh number and aspect ratio.

based on the definition from Thomas and de Vahl Davis[3]: a conduction regime and a boundary-layer regime. However, for $H = 17.31$, $K = 6.43$ and $H = 10.65$, $K = 9.86$, it is only the boundary-layer regime that is identified. This finding is in general the same as that of Refs. 1 and 2. However, one may find that the heat-transfer data of the current form have values lower than those from Bhushan et al.[2] but higher than those from Sheriff[6] at the same H and K values. In addition, the onset of the boundary-layer regime starts at a lower Ra than that found by previous investigators. Moreover, according to the results from flow visualizations, one may find that the conduction regime can be clearly observed for the case of $H = 37.71$ and $K = 3.50$. However, for the cases of $H = 17.31$, $K = 6.43$ and $H = 10.65$, $K = 9.86$, it seems that the conduction regime is difficult to identify. This indicates that the current boundary condition does affect the flow pattern somehow.

In view of the foregoing discussion, the following correlation equation for the boundary-layer regime is obtained from the multiple regression analysis for $Nu = CRa^nH^m$ as

$$Nu = 0.191Ra^{0.3204}H^{-0.121} \tag{13}$$

within $\pm 3\%$ of the original data. This correlation is shown in Fig. 11 and is verified by the current scale analysis. Although Boussinesq approximation ($\Delta T \sim 10^\circ$C) was applied to the current scale analysis, average temperature differences of inner and outer cylinders were found to be about 30–40°C or even larger in all the experimental runs. Nevertheless, the argument drawn from the analysis may still stand for the present experimental results for a qualitative verification.

Conclusion

The correlations obtained in the present work show that the average Nusselt number in tall vertical annuli with the inner wall at constant heat flux and the outer wall cooled to the ambient is strongly dependent on the geometry of the system. This finding agrees favorably with the results of previous investigations. A scale analysis with a proposed thermal boundary thickness was obtained and examined with the final result. Flow visualization was made for different Ra, H, and K, and two different flow regimes were identified. The present results show that the cold-wall boundary condition has a significant effect upon the flow pattern and overall heat transfer for the onset of transition from conduction regime to boundary-layer regime and for the magnitude of the heat-transfer coefficient.

References

[1]Keyhani, M., Kulacki, F. A., and Christensen, R. N., "Free Convection In a Vertical Annulus With Constant Heat Flux On the Inner Wall," *Journal of Heat Transfer*, Vol. 105, Aug. 1983, pp. 454–459.

[2]Bhushan, R., Keyhani, M., Christensen, R. A., and Kulacki, F. A., "Correlation for Convection Heat Transfer In Vertical Annular Gas Layers With Constant Heat Flux On the Inner Wall," *Journal of Heat Transfer*, Vol. 105, Nov. 1983, pp. 910–912.

[3]de Vahl Davis, G. and Thomas, R. W., "Natural Convection Between Concentric Vertical Cylinder," *High Speed Computing in Fluid Dynamics, Physics of Fluids*, Supplement II, Jan. 1969, pp. 198–207.

[4]Thomas, R. W. and de Vahl Davis, G., "Natural Convection In Annular and Rectangular Cavities—A Numerical Study," *Proceedings of the 4th International Heat Transfer Conference*, Vol. 4, Paper NC 2.4, Elsevier, Amsterdam, 1970.

[5]Nagendra, H. R., Tirunarayanan, M. A., and Ramachandran, A., "Free Convection Heat Transfer In Vertical Annuli," *Chemical Engineering Science*, Vol. 25, 1970, pp. 605–610.

[6]Sheriff, N., "Experiment Investigation of Natural Convection In Single and Multiple Vertical Annuli With High Pressure Carbon Dioxide," *Proceedings of the 3rd International Heat Transfer Conference*, Chicago, 1966, pp. 132–138.

[7]Choi, I. G. and Korpela, S. A., "Stability of the Conduction Regime of Natural Convection In a Tall Vertical Annulus," *Journal of Fluid Mechanics*, Vol. 99, Pt. 4, 1980, pp. 725–738.

[8]Figliola, R. S., "Convection Transitions Within a Vertical Cylinder Heated From Below," *Physics of Fluids*, Vol. 29, Aug. 1986, pp. 2028–2031.

[9]Bejan, A., *Convection Heat Transfer*, Wiley-Interscience, New York, 1984, pp. 160–164.

[10]Holman, J. P., *Heat Transfer*, 5th ed. McGraw-Hill, New York, 1981, pp. 336–337.